Nanotribological Properties of Alkanephosphonic Acid Self-Assembled Monolayers on Aluminum Oxide: Effects of Fluorination and Substrate Crystallinity

Matthew J. Brukman,[†,‡] Gerard Oncins Marco,[§] Timothy D. Dunbar,[#] Larry D. Boardman,[#] and Robert W. Carpick*[,†]

Department of Engineering Physics, University of Wisconsin, Madison, Wisconsin 53706, Department of Physical Chemistry, University of Barcelona, Barcelona, Spain, and 3M Corporate Research Materials Laboratory, St. Paul, Minnesota 55144

Received October 22, 2005. In Final Form: January 12, 2006

Two phosphonic acid (PA) self-assembled monolayers (SAMs) are studied on three aluminum oxide surfaces: the C and R crystallographic planes of single crystal α-alumina (sapphire) and an amorphous vapor-deposited alumina thin film. SAMs are either fully hydrogenated $CH_3(CH_2)_{17}PO_3H_2$ or semifluorinated $CF_3(CF_2)_7(CH_2)_{11}PO_3H_2$. Atomic force microscope (AFM) topographic imaging reveals that the deposited films are homogeneous, atomically smooth, and stable for months in the laboratory environment. Static and advancing contact angle measurements agree with previous work on identical or similar films, but receding measurements suggest reduced coverage here. To enable reproducible nanotribology measurements with the AFM, a scanning protocol is developed that leads to a stable configuration of the silicon tip. Adhesion for the semifluorinated films is either comparable to or lower than that for the hydrogenated films, with a dependence on contact history observed. Friction between each film and the tips depends strongly upon the type of molecule, with the fluorinated species exhibiting substantially higher friction. Subtle but reproducible differences in friction are observed for a given SAM depending on the substrate, revealing differences in packing density for the SAMs on the different substrates. Friction is seen to increase linearly with load, a consequence of the tip's penetration into the monolayer.

Introduction

Self-assembled monolayers (SAMs) have aroused great interest as a means of tailoring surfaces for micro- and nanoscale applications including biosensing,[1] stiction reduction,[2] micro- and nanolithography,[3] and corrosion resistance.[4] The most widely researched SAM precursor is the alkanethiol,[5] which is effective in reducing adhesion and friction on noble metals, particularly gold, but substrates for high-quality alkanethiol self-assembly are largely limited to these noble metals. Even on gold, the sulfur headgroup atom that binds it to the substrate will oxidize with time, leading to degradation of the corresponding tribological properties[6] in the absence of replenishing vapor- or liquid-phase molecules. Because strategies for nanotechnology typically include silicon lithography processes and new techniques that use other novel materials, it is critical to develop stable SAMs suitable for a wide range of native metal and semiconductor oxides. Two such materials are phosphonic acid (PA) and silane SAMs. The latter presents certain challenges in its deposition and surface attachment.[7,8] PA SAMs, however, form robust attachments to most metal oxides and are thus excellent candidates for a wide array of substrates.[9]

The alkanephosphonic acid molecule $CH_3(CH_2)_nPO_3H_2$ is a linear hydrocarbon chain with a phosphonic acid headgroup (P tetrahedrally bonded to C, O, and two OH groups) at the terminus. The headgroup is expected to bind to an oxide surface via two or three condensate bonds to surface oxygen atoms. Two species of alkanephosphonic acid are used in this investigation—one with a true alkane chain, $CH_3(CH_2)_{17}PO_3H_2$ (denoted $H_{18}PA$), and one fluorinated at the tail end, $CF_3(CF_2)_7(CH_2)_{11}PO_3H_2$ ($F_8H_{11}PA$). In a recent study, the identical semifluorinated molecule and fully alkane versions with either 16- or 22-carbon atoms were shown to form well-ordered monolayers on the native oxide of Al.[10]

Previous experimental and molecular dynamics studies have shown that other SAMs with terminal fluorine groups have surface properties distinct from those of fully hydrogenated SAMs.[11,12] Fluorinated SAMs are more hydrophobic and are superior electrical barriers compared to hydrogenated monolayers.[13] However, the nanoscale frictional forces measured against these surfaces are also significantly higher.[14,15] The fluorinated portion of a SAM molecule like $F_8H_{11}PA$ is also structurally different from that of an alkane chain. In the latter, the carbon backbone defines a single plane in the trans configuration. In $(CF_2)_n$ chains, however, the carbon atoms form a helix. Replacing H with F also

* Corresponding author. E-mail: carpick@engr.wisc.edu. Fax: +1 608-263-7451.
§ University of Barcelona.
# 3M Corporate Research Materials Laboratory.
† University of Wisconsin.
‡ Currently at North Carolina State University, Department of Physics.

(1) Chaki, N. K.; Vijayamohanan, K. *Biosens. Bioelectron.* **2002**, *17*, 1−12.
(2) Ashurst, W. R.; Yau, C.; Carraro, C.; Lee, C.; Kluth, G. J.; Howe, R. T.; Maboudian, R. *Sens. Actuators, A* **2001**, *91*), 239−248.
(3) Friebel, S.; Aizenberg, J.; Abad, S.; Wiltzius, P. *Appl. Phys. Lett.* **2000**, *77*, 2406−2408.
(4) Whelan, C. M.; Kinsella, M.; Carbonell, L.; Ho, H. M.; Maex, K.*Microelectron. Eng.* **2003**, *70*, 551−557.
(5) Nuzzo, R. G.; Allara, D. L. *J. Am. Chem. Soc.* **1983**, *105*, 4481−4483.
(6) Kiely, J. D.; Houston, J. E. *Langmuir* **1999**, *15*, 4513−4519.
(7) Legrange, J. D.; Markham, J. L.; Kurkjian, C. R. *Langmuir* **1993**, *9*, 1749−1753.
(8) Stevens, M. J. *Langmuir* **1999**, *15*, 2773−2778.
(9) van Alsten, J. G. *Langmuir* **1999**, *15*, 7605−7614.
(10) Pellerite, M. J.; Dunbar, T. D.; Boardman, L. D.; Wood, E. J. *J. Phys. Chem. B* **2003**, *107*, 11726−11736.
(11) Gao, J. P.; Luedtke, W. D.; Gourdon, D.; Ruths, M.; Israelachvili, J. N.; Landman, U. *J. Phys. Chem. B* **2004**, *108*, 3410−3425.
(12) Briscoe, B.; Evans, D. *Proc. R. Soc. London, Ser. A* **1982**, *380*), 389−407.
(13) Chidsey, C. E. D.; Loiacono, D. N. *Langmuir* **1990**, *6*, 682−691.
(14) Kim, H. I.; Koini, T.; Lee, T. R.; Perry, S. S. *Langmuir* **1997**, *13*, 7192−7196.
(15) DePalma, V.; Tillman, N. *Langmuir* **1989**, *5*, 868.

10.1021/la052847k CCC: $33.50
Published on Web 03/23/2006

increases the size of the individual molecules. Fluorinated chain segments have a van der Waals radius of 0.567 nm,[16] whereas the corresponding value for alkyl segments is 0.424 nm.[17] Structural differences between CH_2 and CF_2 chains make the latter stiffer, increasing the elastic modulus.[18−22] The mechanism(s) by which fluorinated SAMs exhibit greater shear strength (or friction) is not yet understood; candidate phenomena include packing[23] and changes in characteristic activation volumes,[12] while adhesion effects have been ruled out.[24]

The commercial availability of synthetic single crystal α-alumina (sapphire) with flat, oriented crystal faces, and the ease of depositing smooth films of amorphous alumina allow for a straightforward investigation of the dependence of monolayer quality on substrate surface crystallinity. The question of surface crystallinity occurs on two levels: First, either the surface is amorphous or crystalline. Then, if it is crystalline, the differences between crystallographic planes can be examined. The (1000) and ($1\bar{1}02$) planes, also known respectively as the C and R planes,[25−27] are used here in addition to an amorphous aluminum oxide thin film. The C-plane surface consists of hexagonally spaced oxygen atoms, packed three per unit mesh, which is a rhombus of area 0.196 nm^2. The R-plane unit mesh is rectangular and occupies 0.244 nm^2. In this mesh, two oxygen atoms lie on the surface with two more lying slightly lower but still exposed. These are shown in Figure 1 (adapted from Guo et al.[25]). The vapor-deposited alumina is expected to be amorphous without any long-range ordering of oxygen atoms.

Experimental Section

Substrates to be coated with SAMs were prepared as follows. Single crystal C- and R-plane sapphire crystals (MarkeTech International, Port Townsend, WA) were cleaned with piranha solution (4:1 H_2SO_4:H_2O_2 30% in H_2O) then annealed at 1300 °C for 48 h, then rinsed with ethanol. Piranha tends to leave oxide surfaces clean of hydrocarbons and well hydroxylated. It is very reactive with organic materials and should be used with great care. Alumina-coated (150 nm) Si (100) wafers (Silicon Valley Microelectronics, San Jose, CA) were rinsed with heptane, acetone, and 2-propanol, blown dry with N_2, and exposed to ultraviolet light (ozone cleaning) for 10 min. The amorphous and crystalline substrates were then immersed in 1 mM $F_8H_{11}PA$ or $H_{18}PA$ ethanol solutions for 24 h and rinsed with ethanol. Uncoated (blank) C- and R-plane sapphire dies were also piranha cleaned and ethanol rinsed and then annealed at 1300 °C shortly before initial AFM imaging. All samples were rinsed with ethanol again immediately before their initial imaging in the AFM.

Contact angles measurements with water and hexadecane were performed with an AST Products (Billerica, MA) VCA-2500XE video contact angle measurement apparatus. Drop volumes were 5 μL for static and 3−7 μL for the dynamic angle measurements in which fluid was added (advancing) or removed (receding) from the droplet. Reported here are average contact angles for at least two different samples of the same type. Hexadecane static measurements were indistinguishably close to advancing values and are not reported. Uncertainties in the contact angles are estimated to be ±2° for static and advancing angle measurements and ±5° for receding angle measurements. After contact angle measurements, all samples were washed with heptane and 2-propanol and blown dry with N_2.

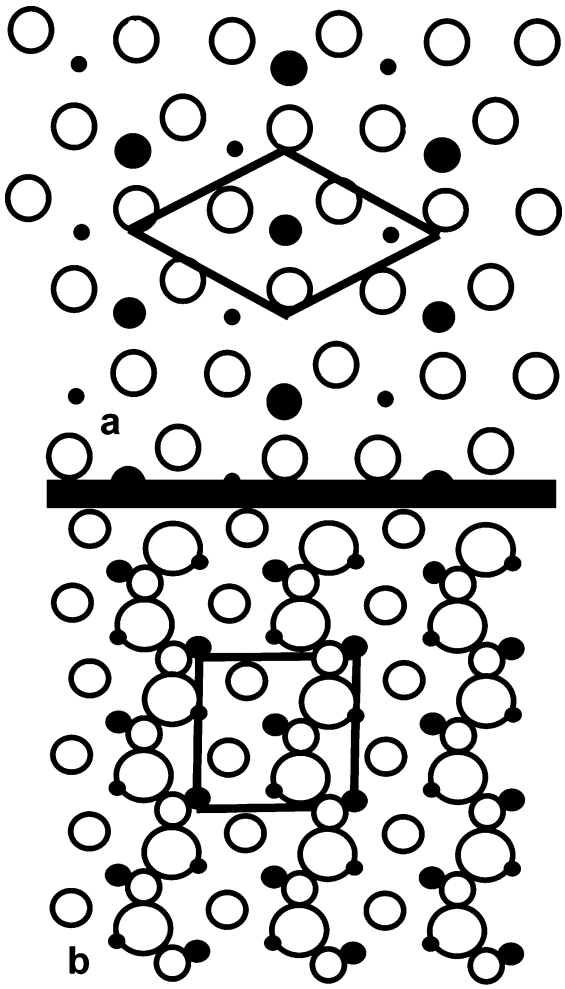

Figure 1. C plane (a) and R plane (b) surfaces, adapted from Ref. 25. Repeating mesh units are indicated by solid lines, oxygen by open circles, and aluminum by solid circles. Increased size indicates proximity to the surface.

Atomic force microscopy was performed with a Digital Instruments Multimode AFM with a Nanoscope IV controller. The instrument was placed on a vibration isolation platform and under a foam sound-absorbing hood in the ambient atmosphere with the temperature consistently 20−22 °C. The relative humidity varied from day to day, but preliminary work has shown that varying the humidity from 5 to 60% does not have a noticeable effect on friction or adhesion for these PA SAMs. The surfaces of both monolayers are hydrophobic, so water should not be strongly adsorbed to the surface at low to moderate ambient humidity.

Cantilevers were rectangular Si with its native oxide (Mikromasch, nominal dimensions 35 μm × 300 μm, nominal spring constant 0.2 N/m). Each lever's normal force constant was calibrated experimentally by Sader's unloaded resonance method,[28] with the plan view dimensions measured with the eyepiece of a Beuhler Micromet microindenter (Lake Bluff, IL). The lateral force calibration for

(16) Brandrup, J.; Immergut, E. H. *Polymer Handbook*, 2nd ed.; Wiley: New York, 1975.
(17) Tamada, K.; Nagasawa, J.; Nakanishi, F.; Abe, K.; Hara, M.; Knoll, W.; Ishida, T.; Fukushima, H.; Miyashita, S.; Usui, T.; Koini, T.; Lee, T. R. *Thin Solid Films* **1998**, *329*, 150−155.
(18) Gallaher, K. L.; Yokozeki, A.; Bauer, S. H. *J. Phys. Chem.* **1974**, *78*, 2389−2395.
(19) Wolf, S. G.; Deutsch, M.; Landau, E. M.; Lahav, M.; Leiserowitz, L.; Kjaer, K.; Alsnielsen, J. *Science* **1988**, *242*, 1286−1290.
(20) Naselli, C.; Swalen, J. D.; Rabolt, J. F. *J. Chem. Phys.* **1989**, *90*, 3855−3860.
(21) Eaton, D. F.; Smart, B. E. *J. Am. Chem. Soc.* **1990**, *112*, 2821−2823.
(22) Barton, S. W.; Goudot, A.; Bouloussa, O.; Rondelez, F.; Lin, B. H.; Novak, F.; Acero, A.; Rice, S. A. *J. Chem. Phys.* **1992**, *96*, 1343−1351.
(23) Overney, R. M.; Meyer, E.; Frommer, J.; Brodbeck, D.; Lüthi, R.; Howald, L.; Güntherodt, H.-J.; Fujihara, M.; Takano, H.; Gotoh, Y. *Nature* **1992**, *359* (6391), 133.
(24) Chaudhury, M. K.; Owen, M. J. *Langmuir* **1993**, *9*, 29−31.
(25) Guo, J.; Ellis, D.; Lam, D. *Phys. Rev. B* **1992**, *45*, 13647−13656.
(26) Hongo, H.; Yudasaka, M.; Ichihashi, T.; Nihey, F.; Iijima, S. Chemical vapor deposition of single-wall carbon nanotubes on iron-film-coated sapphire substrates. *Chem. Phys. Lett.* **2002**, *361*, 349−354.
(27) Guo, J.; Ellis, D. E.; Lam, D. J. *Phys. Rev. B* **1992**, *45*, 3204−3214.
(28) Sader, J.; Chon, J.; Mulvaney, P. *Rev. Sci. Instrum.* **1999**, *70*, 3967−3969.

each cantilever, measured via the wedge method,[29,30] was performed using a calibration grating (Mikromasch TGG01) providing two facets oriented at a known dihedral angle. Open-source Matlab scripts[31] were used to extract and average the optical sensitivity (photodetector signal volts/nm of cantilever motion) from batches of force−distance curves and to generate the data plots required for the calibration calculations. The scripts were also used to generate individual force-calibrated friction-load data sets from the raw Nanoscope output files.

For friction versus load (FL) studies, a slowly descending sawtooth waveform from an external function generator was added to the setpoint signal (at the Quadrex board of the Nanoscope IV controller), allowing the feedback control to continuously decrease the normal force over the course of an image. The FL images were 25 nm scans (perpendicular to the long axis of the cantilever) acquired at 6.1 Hz, with 512 lines and 512 pixels per line, corresponding to a scan velocity of 152.5 nm/s. Although the slow scan axis was turned off, there was still considerable tip motion longitudinally (along the surface parallel to the long axis of the cantilever) due to the intrinsic geometric coupling between the vertical and longitudinal displacement of the tip relative to the sample created by the tilt angle of the cantilever.[32,33] Depending on the load range for a given FL measurement, this total longitudinal tip displacement was never more than 200 nm. As discussed below, the samples were sufficiently homogeneous that this had no effect on the measurements. Imaging the selected region before and after the measurements ensured that step edges and any other defects were avoided during FL measurements.

Initially, the frictional force between the tip and sample changed as measurements were repeated under otherwise identical conditions. This could be explained only by the transfer of molecules from the SAM to the tip, a phenomenon that has been observed previously for silane films.[34] This necessitated a run-in procedure to stabilize the tip. A steady-state tip surface was attained by scanning the tip against the SAM at appreciable loads (50 to 100 nN) on the sample before performing FL measurements. New regions of the sample were always used for measurements after the tip treatment procedure was carried out. This is similar to a previously reported method of tip treatment[34] by scanning the tip against a mica sample, except that here the sample used for treatment and measurement is the same. A comprehensive discussion of the tip treatment process, including a demonstration of the tip contamination that it remedies, is presented in the Results section.

Friction forces were determined in the standard manner by taking the half-width of the trace−retrace friction loops for each fast-scan line of the image, averaged over the center 256 pixels of each 512-pixel line to avoid the sticking portion of the loop. The normal load signal was similarly averaged. Because the setpoint was varied continuously, the corresponding uncertainty associated with the normal force for each point in a given FL experiment is 1/1700th of the total range of the peak-to-peak force for that trace. Ten to 20 friction-load images were taken per sample: 5 to 10 at one location and an equal number at another location a few hundred nanometers away. Averages of the friction-load measurements were determined by combining data sets from a given location, sorting by the normal force, and averaging the normal and frictional forces in groups of consistent ranges of normal force. The 95% confidence intervals within the groups of 10 were generally less than 0.1 nN in normal force and $<10\%$ of the average lateral force for each group.

Except at loads just greater than the pull-off load, individual friction-load measurements were essentially linear. This is in contrast to the numerous observations of nonlinear friction-load behavior for solid−solid interfaces.[35,36] This has been attributed to a direct dependence of friction upon the contact area, which varies with load in a nonlinear fashion because of elastic deformation. Without further information about the contact area, we are unable to connect the interfacial shear strength (frictional force per unit area) directly to the frictional force, although the linear dependence is suggestive of either a linear pressure dependence of the shear strength[11,12] or the fact that the frictional force is not primarily related to the interfacial contact area. This will be revisited in the Discussion section. A useful metric for comparing the frictional properties of the surfaces is the slope of the FL traces, which we denote as α, having the physical interpretation of the average differential friction for a given FL measurement or "single-asperity friction coefficient."

Another metric of interest is the pull-off force between the tip and sample. This was determined both from force−distance (FD) curves, in which the sample is raised into contact with the tip and then withdrawn, and from the FL measurements previously described. In both types of measurement, the pull-off force was taken to be the difference in normal force between the unloaded out-of-contact position and the last data point acquired before the tip pulls out of contact with the sample. FD and FL measurement procedures are different in that FDs are much shorter in duration (total time per measurement: 0.5 versus 85 s) and involve less sliding because the tip is not being scanned laterally during the measurement.

Several cantilevers were used in these experiments to establish reproducibility. The tip of each lever was imaged by shadow transmission electron microscopy before use in the AFM to ensure that the tip shape was well defined and smoothly curved, and had a small radius of curvature. Initially having radii of curvature of 20 nm or less, they were worn to radii of up to 47 nm[37] over the course of the hours of sliding contact involved in a given experiment. This effect was anticipated and was accounted for by cycling through all of the samples twice in a given experiment. Thus, the first measurements could be compared to those taken on the same sample hours later. Whereas pull-off forces tended to increase with tip use, the friction measurements, particularly the slopes of the FL plots, were very consistent for a given sample and are used as the figures of merit in quantifying friction. Although the meaning of the slope will be explained in the Discussion section, it is worth emphasizing here that the slopes α were not affected by these changes in tip radius.

Each sample was imaged topographically before friction measurements were performed. Both SAM-coated C-plane and blank C-plane sapphire substrates had wide terraces approximately 1.4 nm in height, corresponding well to the 1.3 nm separation of the basal planes of the lattice (Figure 2). Topographs of the monolayer on the R plane (Figure 3) also showed a distribution of step heights in the 1−2 nm range (1.2 nm steps are expected). Excess PA SAM molecules or other loosely bound contaminants were easily swept away by taking a topographic image at low loads ($\sim$20−30 nN). The coated amorphous alumina surfaces were much more uniform, with reduced topographic variation and no indication of excess PA molecules (Figure 4). That there was no excess material evident in the C-plane and amorphous alumina topographs suggests that PA SAM deposition was more uniform on those surfaces than on the R plane. For all samples, the rms roughness was less than 0.5 nm for an image size of 1 μm^2 (multiple terraces in the image) or smaller and less than 0.1 nm for (100 nm)^2, corresponding to a single terrace.

Results

A. Contact Angle. Contact angle measurements were performed to determine the wettability of the SAMs with polar (water) and nonpolar (hexadecane) liquids. Small contact angles

(29) Varenberg, M.; Etsion, I.; Halperin, G. *Rev. Sci. Instrum.* **2003**, *74*, 3362−3367.

(30) Ogletree, D.; Carpick, R.; Salmeron, M. *Rev. Sci. Instrum.* **1996**, *67*, 3298−3306.

(31) The scripts are available for noncommercial use at http://mandm.engr.wisc.edu/faculty_pages_carpick/toolbox.htm.

(32) Cannara, R. J.; Brukman, M. J.; Carpick, R. W. *Rev. Sci. Instrum.* **2005**, *76*, 53706-1-6.

(33) Watson, G. S.; Dinte, B. P.; Blach-Watson, J. A.; Myhra, S. *Appl. Surf. Sci.* **2004**, *235*, 38−42.

(34) Qian, L. M.; Xiao, X. D.; Wen, S. Z. *Langmuir* **2000**, *16*, 662−670.

(35) Enachescu, M.; van den Oetelaar, R.; Carpick, R.; Ogletree, D.; Flipse, C.; Salmeron, M. *Tribol. Lett.* **1999**, *7*, 73−78.

(36) Carpick, R.; Ogletree, D.; Salmeron, M. *J. Colloid Interface Sci.* **1999**, *211*, 395−400.

(37) The "after" radii were estimated via the lateral calibration sample. Topographs of the crests of the wedge grating provided an upper bound to the sharpness of the tip. Radii were calculated by fitting parabolas to the topographs $\pm$45 nm on either side of the crest.

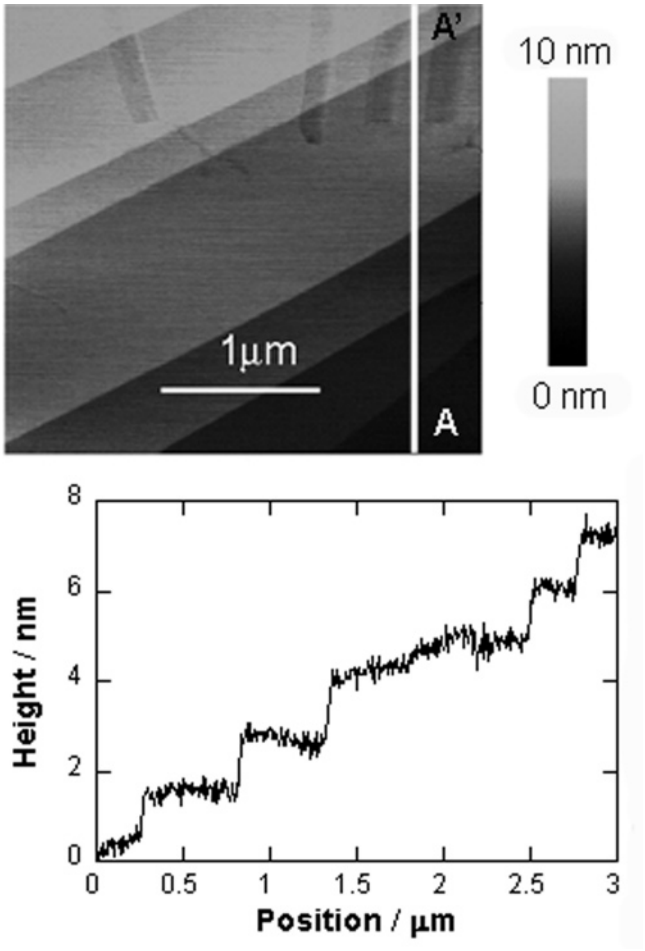

Figure 2. AFM topographic image and cross-sectional profile (from A to A′) of $H_{18}PA$ on C-plane sapphire. Adjacent terraces differ in height by 1.2 nm.

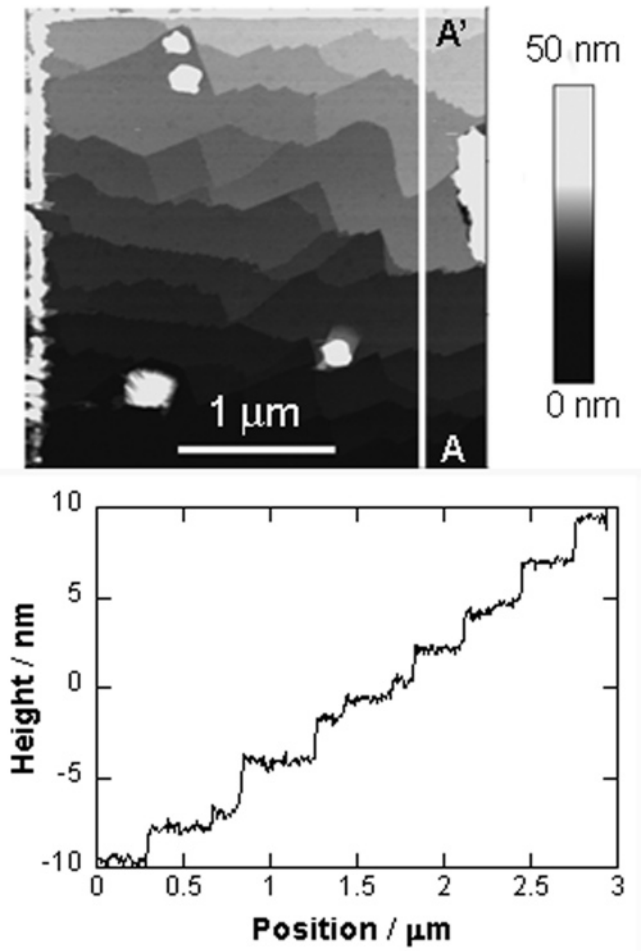

Figure 3. AFM topographic image and cross-sectional profile (from A to A′) of $H_{18}PA$ on R-plane sapphire after excess coating (visible as the white bands at the left and top) has been swept aside.

indicate the spreading of the fluid on the SAM whereas large angles indicate that contact between the fluid and SAM is unfavorable. As expected, and without regard to the underlying Al_2O_3 surface, the $F_8H_{11}PA$ SAMs always exhibited greater contact angles with water and hexadecane than did the $H_{18}PA$ SAMs (Tables 1 and 2). Interestingly, there was also less variation for a given contact angle measurement among the three types of alumina for $H_{18}PA$ than for $F_8H_{11}PA$. The variation between substrates within four of the five measurements for each hydrogenated PA was less than the variation in the semifluorinated PA, with the exception being the advancing hexadecane measurement.

B. Tip Contamination. Our initial measurements showed a considerable amount of transient behavior within a set of FL measurements, especially when switching between $H_{18}PA$ and $F_8H_{11}PA$ samples. Tip contamination by the SAM molecules was believed to be the cause, and this was confirmed more directly by scanning an uncoated alumina sample after scanning a SAM-coated sample and observing even more pronounced transient effects. Figure 5 demonstrates the variation in friction as material is added to and then removed from the tip, depending on the sample being scanned. The first FL measurement shown (labeled "0") was obtained with a fresh tip on bare alumina. Subsequently, a series of FL measurements were performed on an $H_{18}PA$ monolayer (not shown; see further below for a comparison of frictional forces between coated and uncoated samples). FL data were immediately taken again on the same alumina surface (chronologically labeled 1−8).

Table 1. Water and Hexadecane Contact Angle Measurements on the $H_{18}PA$ SAM

	water	hexadecane
alumina type	adv/static/rec	adv/rec
C-plane sapphire	111°/106°/80°	41°/37°
R-plane sapphire	112°/106°/82°	39°/36°
amorphous Al_2O_3	114°/109°/89°	38°/31°

Table 2. Water and Hexadecane Contact Angle Measurements on the $F_8H_{11}PA$ SAM

	water	hexadecane
alumina type	adv/static/rec	adv/rec
C-plane sapphire	121°/111°/82°	80°/77°
R-plane sapphire	122°/108°/83°	80°/73°
amorphous Al_2O_3	126°/121°/109°	81°/69°

Friction is seen to be greatly reduced at first but then increases with time. This transient behavior can be explained only by material transfer from the $H_{18}PA$ surface to the tip (between runs 0 and 1) and subsequent removal from the tip by scanning the high-friction bare surface (during scans 1−8). The general implications of this behavior are very important if accurate and reproducible friction measurements with AFM are desired: the tip chemistry may change upon scanning a new sample, and the tip must be brought to steady state before measurements can be considered trustworthy. The extent to which transient frictional behavior occurs may also be a general, qualitative indication of the bonding of SAM molecules to a substrate.

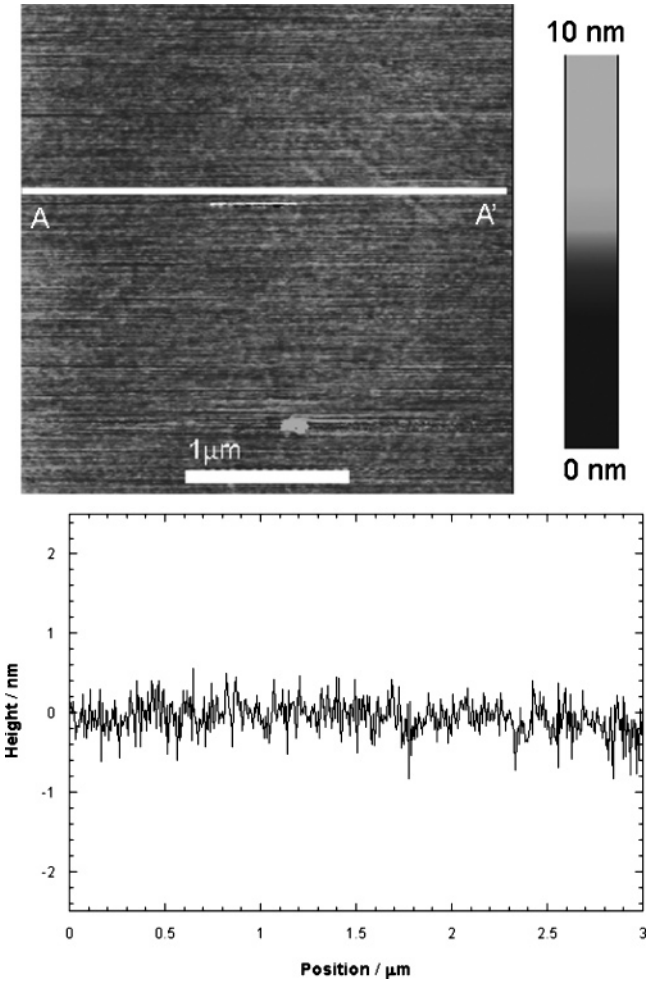

Figure 4. AFM topographic image and cross section (from A to A′) of the $F_8H_{11}PA$ SAM on amorphous alumina.

The purpose of the run-in procedure discussed in the Experimental Section is not necessarily to remove material from the tip but to replace material on the tip until it reaches a steady state for that particular surface. The configuration of the material on the tip is simply not known and is extremely difficult to characterize. (There are no established methods for this.) A simple schematic is shown in Figure 6. The primary consequence of this equilibration procedure is that friction and adhesion measurements presented here are not tip-on-SAM but $H_{18}PA$-on-(defective)-$H_{18}PA$ or $F_8H_{11}PA$-on-(defective)-$F_8H_{11}PA$. In other words, we are studying friction, adhesion, and contact evolution processes that are relevant when an uncoated asperity makes contact with a SAM-coated surface. Also, previous friction measurements performed on other SAMs without any confirmation of stable, reproducible behavior may warrant reinterpretation in light of these results on phosphonic acid SAMs.

C. Adhesion. Adhesion measurements were obtained in a number of different sessions of data acquisition. There were large variations in pull-off force measurements, and this occurred on four levels of descending magnitude: (level 1) from experiment to experiment involving different tips, (level 2) from position to position on the same sample during a single experiment using the same tip, (level 3) from one type of measurement to the other (FD or FL), and (level 4) from one type of monolayer ($F_8H_{11}PA$ vs $H_{18}PA$) to the other.

The variation within level 1 is illustrated in the bar graph plot of Figure 7, which shows the variation in pull-off force measured on different days and with different AFM cantilevers/tips,

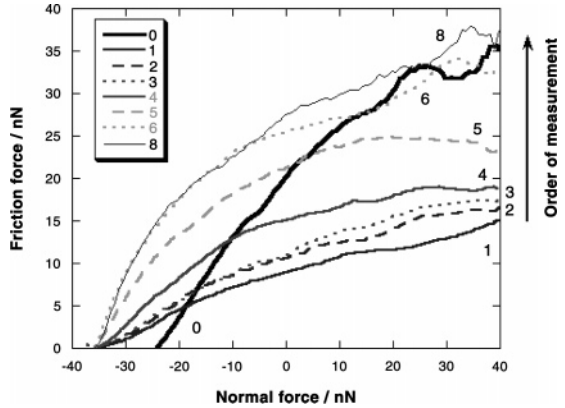

Figure 5. FL measurements on bare amorphous alumina. 0 (solid line) is the response of an unused tip on the bare alumina sample. Then, the tip was scanned on an $H_{18}PA$ sample (acquired data not shown). Subsequent scans (1−8, in order of acquisition) show the response of this used tip on the bare alumina sample again. The frictional forces at each normal force increase with successive measurements, eventually reaching steady state, similar to the original measurement 0, as the SAM molecules are removed from the tip. The larger adhesion force seen in 8 as compared with that in 0 can be explained by an increase in the tip radius. Data set 7 overlapped sets 6 and 8 and is not shown for clarity.

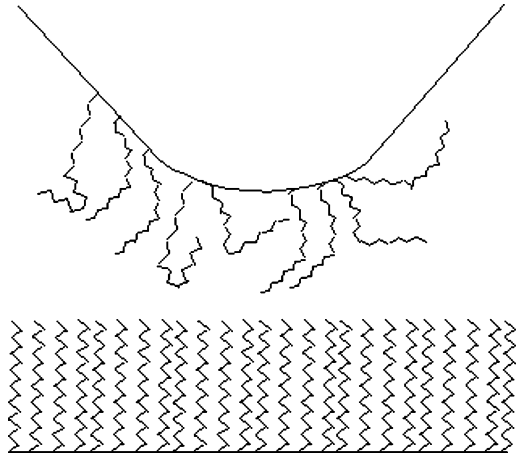

Figure 6. Simple schematic illustrating molecules transferred to the tip. Adsorbed SAM molecules may lie on the surface or may attach to the tip via end groups.

expressed in terms of the work of adhesion, calculated according to DMT contact mechanics.[38] The post-scanning (blunted) tip radii were used for the calculations, so these values represent lower bounds to the work of adhesion. This is aggregate data for all types of alumina substrates because there was little variation in adhesion among the three types of substrates with the same type of SAM on a given day. Approximately equal numbers of measurements were taken for each PA/substrate combination, and the measurements are shown in chronological order.

With tips 0 and 3, $F_8H_{11}PA$ and $H_{18}PA$ are indistinguishable. From the second and third data sets, each taken with tip 2 but separated by 12 h, the $H_{18}PA$ shows distinctly higher adhesion, with the adhesion between $F_8H_{11}PA$ and the tip approximately 55% that of $H_{18}PA$. The laboratory's relative humidity readings during the measurements were as follows: tip 1 = 20%; tip 2, session 1 = 42%; tip 2, session 2 = 45%; tip 3 = not known but believed to be 40−50% on the basis of the consistent known behavior of the laboratory.

(38) Derjaguin, B. V.; Muller, V. M.; Toporov, Y. P. *J. Colloid Interface Sci.* **1975**, *53*, 314−326.

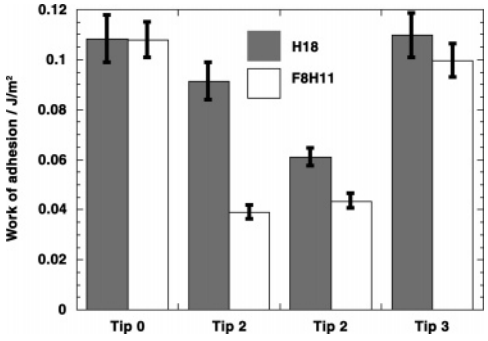

Figure 7. Adhesion measurements of PA SAM films on alumina, measured with a silicon AFM tip. Only one tip was used per pair of data columns. Error bars are 95% confidence intervals. For the four sets of measurements, $N = 250$, 105, 105, and 240, respectively.

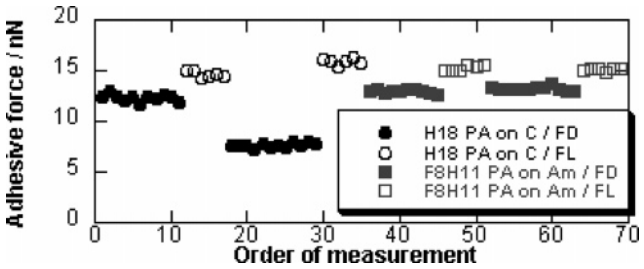

Figure 8. Pull-off force as measured by both force−distance curves and from FL measurements. Adhesion was usually greater during friction measurements and tended to increase with time within a given series of measurements, suggesting that adhesion hysteresis is playing a role.

Levels 2 and 3 of variation (local spatial variation and differences between FD and FL measurements) are evident in the scatter plot of Figure 8 with FD and FL data obtained at two distinct locations from each other, each for $H_{18}PA$ and $F_8H_{11}PA$. FL measurements clearly and consistently yield greater pull-off forces than FD tests. (Data in this Figure are presented in terms of the raw pull-off force rather than the work of adhesion.) Because transfer of material from the SAM to the tip is observed, it is suspected that increased deformation of the tip and sample chain molecules,[39,40] which is facilitated by the increased contact times and compressive nature of the FL measurement, is the cause of this difference between FD and FL measurements.

This difference between FD and FL pull-off forces is consistent with the "adhesion hysteresis" idea of Israelachvili,[41,42] who showed that increased contact time and load for chainlike molecules lead to greater pull-off forces. Indeed, the tip and SAM are in contact for much longer times and sliding distances during FLs (85 s, 26 μm) than during FDs (0.5 s, <200 nm). The difference does not result from the different loading rates used because 0.1 Hz FD measurements showed no difference with FD measurements taken at 2 Hz. Also, in one particular instance, moving from one position to another in the $H_{18}PA$ results in the FD pull-off force being reduced, whereas the FL data remain in relative agreement with those from the previous spot, demonstrating the position-to-position variation in pull-off force. It is possible that the variations could reflect local differences in the SAM packing density, but if so, it is surprising that the FL data were not affected; we therefore suggest that this is unlikely. The variations in pull-off force that we observe require further study that involves the extremely challenging task of identifying the specific chemical nature of the tip as well as its shape and size; they may also reflect local surface or tip contamination.

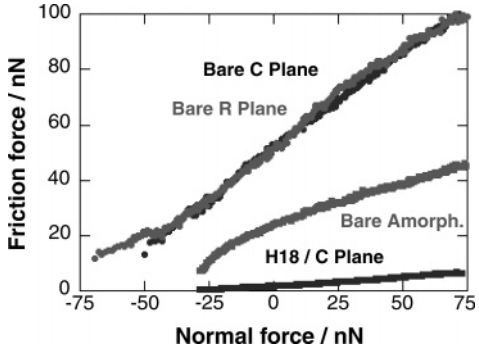

Figure 9. Friction versus load for three bare alumina surfaces and an $H_{18}PA$ film. Each data set represents an average of 10 measurements. Friction for the bare amorphous surface is lower than for the bare crystalline surfaces, likely because of increased ambient contamination because this surface was not furnace annealed. All SAM-coated surfaces, including the one shown here, exhibit friction that is dramatically lower than that for all uncoated surfaces.

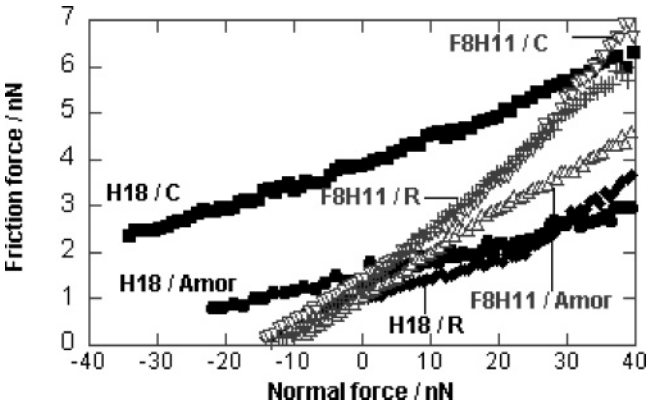

Figure 10. Averages of a series of FL measurements; each is an average of six individual measurements. Only one of every five data points is shown for clarity. Standard errors in frictional force (not shown) extend <4% in each direction.

D. Friction. Most dramatically, the application of a PA monolayer to all three types of bare alumina greatly reduced friction; see Figure 9 for an example of $H_{18}PA$ compared with the three bare substrates. These measurements were taken 1 month after the C- and R-plane sapphire surfaces had been annealed and stored in laboratory air, whereas the amorphous alumina was never annealed. The sapphire substrates are expected to have a more polar and hydrophilic hydroxylated surface than the bare amorphous alumina, but the exact state is not known. Correspondingly, the bare amorphous substrate exhibits significantly less friction and adhesion than the two bare sapphire substrates. Nevertheless, the PA SAM-coated surface exhibits even more dramatically reduced friction. This decrease was observed for all SAMs, for which absolute frictional forces decreased by up to a factor of 20 and the differential friction decreased by factors ranging from 5 to 11, compared with the bare substrates.

Friction also varied systematically with SAM type. Figure 10 shows FL data on all six SAM/substrate combinations, acquired with the same tip. Results from complete sets of FL measurements

(39) Nakagawa, T.; Ogawa, K.; Kurumizawa, T. *J. Vacuum Sci. Technol., B* **1994**, *12*, 2215−2218.
(40) Richter, R. P.; Brisson, A. *Langmuir* **2003**, *19*, 1632−1640.
(41) Israelachvili, Adhesion, Friction, and Lubrication of Molecularly Smooth Surfaces. In *Fundamentals of Friction: Macroscopic and Microscopic Processes*; Singer, I. L., Pollock, H. M., Eds.; Kluwer Academic Publishers: Dordrecht, The Netherlands, 1992; Vol. 220, pp 351−385.
(42) Yoshizawa, H.; Chen, Y. L.; Israelachvili, J. *Wear* **1993**, *168*, 161−166.

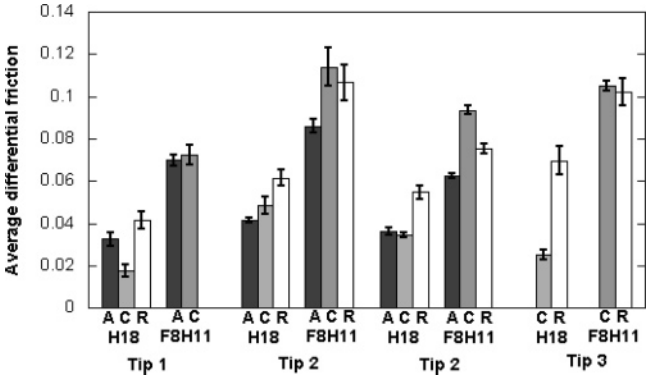

Figure 11. Average differential friction values (α) over a series of measurements involving different tips. (tip 2 was used twice, in the order shown.) A, C, and R correspond to amorphous, C-plane, and R-plane alumina, respectively. Error bars represent 95% confidence intervals. *N* for each tip is 10, 10, 10, and 30.

(all six substrate/SAM combinations) taken with the three tips are shown in Figure 11. Using the average slope of an FL measurement (the single-asperity friction coefficient, α) as the comparative metric, the steeper $F_8H_{11}PA$ curves indicate a larger frictional response for that monolayer as compared to that for $H_{18}PA$. However, larger values of α do not always correspond to larger values of frictional force at a given load because the pull-off force essentially shifts the friction versus load curve to the left. Note that Figure 10 appears to contradict the earlier statement that adhesion does not depend on the substrate, but in fact each FL curve in this example represents only six individual measurements, a small subset of the total number of measurements. As mentioned above, adhesion often varied from location to location and according to the tip condition. Yet surprisingly, these fluctuations in adhesion and, correspondingly, in the frictional force at a given load did not cause α to vary, and we conclude that they do not impede the comparative analysis of the friction measurements. Therefore, we emphasize that our comparisons of frictional response are not necessarily indicative of the magnitude of the frictional force at a given load but rather of the rate of increase of friction with load, which will be discussed further below.

Whereas the absolute slopes α for a given sample changed from tip to tip, they were consistent relative to one another when comparing different samples with the same tip. Specifically, independent of the tip and the adhesion forces, α for $H_{18}PA$ was 30−60% that of α for $F_8H_{11}PA$ on the same substrate. To account for the tip shape and laboratory environment and demonstrate trends among the SAM−substrate pairs, the values of α may be normalized by the value of α of $H_{18}PA$ on the C-plane (α_{CH}) for that session, as shown in Table 3, which reports aggregate data for all tips.

To a lesser extent, α also depended on the type of alumina underneath the SAM. Both $H_{18}PA$ and $F_8H_{11}PA$ monolayers on amorphous alumina (labeled "A" in Figure 11) had a lower α than those on the R sapphire, although for the fluorinated case we were able to make a comparison only between these two substrates for tip 2. The trend was clear and consistent with both sets of measurements using tip 2. $F_8H_{11}PA$ films on amorphous alumina also exhibited α values as low as or lower than those on C-plane sapphire. Comparisons of α for $H_{18}PA$ on C-plane sapphire and amorphous alumina were inconsistent from tip to tip. Furthermore, for $H_{18}PA$ films, the C-plane sapphire exhibited consistently lower α values than the R plane. In contrast, the C and R planes were generally indistinguishable from each other for $F_8H_{11}PA$ SAMs. In summary, we find that the effect of the substrate can be expressed as follows:

Table 3. Values of the Single-Asperity Friction Coefficient Relative to $H_{18}PA$ on the C Plane of Sapphire

SAM/substrate	normalized α (95% confidence)
$H_{18}PA$/C plane	1.0 ± 0.4
$H_{18}PA$/amorphous	1.2 ± 0.1
$H_{18}PA$/R plane	2.2 ± 0.4
$F_8H_{11}PA$/amorphous	2.6 ± 0.2
$F_8H_{11}PA$/R plane	3.2 ± 0.9
$F_8H_{11}PA$/C plane	3.6 ± 0.6

(1) For the $H_{18}PA$ films, we consistently find that $\alpha_A < \alpha_R$ and $\alpha_C < \alpha_R$, but we do not find a consistent, significant difference between α_A and α_C. This indicates that for hydrogenated films the R plane has a modestly unfavorable effect on friction.

(2) For the $F_8H_{11}PA$ films, we consistently find that $\alpha_A < \alpha_C$, although in one of the three cases the difference is not statistically significant. For both sets of measurements with tip 2, we find that $\alpha_A < \alpha_R$. We also find that α_C is either equivalent to or greater than α_R. This indicates that for semifluorinated films the amorphous substrate has a modestly favorable effect on friction.

Discussion

A. Contact Angle and Film Structure. Contact angle measurements, through comparison with previous literature studies, can provide insights into the structure of SAMs. First, we discuss the results for semifluorinated films. Dynamic contact angle data have been reported for $F_8H_{11}PA$ SAMs on the native oxide of vapor-deposited aluminum[10,43] and for $CF_3(CF_2)_7(CH_2)_2$-PO_3H_2 (F_8H_2PA in our shorthand) on vapor-deposited alumina.[44] In accord with those studies and previous studies of similar semifluorinated alkanethiol SAMs on gold,[17,45−47] the advancing and static contact angle data for water and hexadecane reveal that $F_8H_{11}PA$ exposes CF_3 groups to the air/film interface.

The water receding contact angles reported for our semifluorinated films are lower than those reported for $F_8H_{11}PA$ on aluminum's native oxide and for $F_{10}H_{11}SH$ on Au (by ∼10° for amorphous alumina and ∼35° for crystalline), meaning that there is more contact angle hysteresis. Larger hysteresis has been linked to more penetration of the probe liquid into the SAM[48] (e.g., via pinholes in monolayer coverage) and has been reviewed in detail by Chaudhury[49] and references therein. Furthermore, greater hysteresis has been correlated with an increased amount of translational disorder[50] and decreased alkyl chain coverage[51] in alkanethiol SAMs on Au. The lower water contact angle values suggest that our $F_8H_{11}PA$ SAMs have somewhat lower coverage than those prepared on aluminum's native oxide[10] or of $F_{10}H_{11}$-SH on gold.[46] In comparing the data in this study for receding contact angles of water on $F_8H_{11}PA$ on the three substrates, films on R- and C-plane sapphire exhibit smaller advancing contact

(43) We note that those vapor-deposited metal surfaces consist of "irregularly shaped grains...from 0.3 to 1.0 mm" and are much rougher (as measured by AFM) than the alumina or sapphire used here.

(44) Kelley, T. W.; Boardman, L. D.; Dunbar, T. D.; Muyres, D. V.; Pellerite, M. J.; Smith, T. Y. P. *J. Phys. Chem. B* **2003**, *107*, 5877−5881.
(45) Tsao, M.; Hoffmann, C.; Rabolt, J.; Johnson, H.; Castner, D.; Erdelen, C.; Ringsdorf, H. *Langmuir* **1997**, *13*, 4317−4322.
(46) Fukushima, H.; Seki, S.; Nishikawa, T.; Takiguchi, H.; Tamada, K.; Abe, K.; Colorado, R.; Graupe, M.; Shmakova, O. E.; Lee, T. R. *J. Phys. Chem. B* **2000**, *104*, 7417−7423.
(47) Frey, S.; Heister, K.; Zharnikov, M.; Grunze, M.; Tamada, K.; Colorado, R.; Graupe, M.; Shmakova, O. E.; Lee, T. R. *Isr. J. Chem.* **2000**, *40*, 81−97.
(48) Timmons, C. O.; Zisman, W. A. *J. Colloid Interface Sci.* **1966**, *22*, 165−171.
(49) Chaudhury, M. K. *Mater. Sci. Eng., R* **1996**, *16*, 97−159.
(50) Lestelius, M.; Engquist, I.; Tengvall, P.; Chaudhury, M. K.; Liedberg, B. *Colloids Surf., B* **1999**, *15*, 57−70.
(51) Park, J. S.; Vo, A. N.; Barriet, D.; Shon, Y. S.; Lee, T. R. *Langmuir* **2005**, *21*, 2902−2911.

angles and more hysteresis than those on amorphous alumina, meaning that there is higher coverage on the latter, suggesting a higher packing density and perhaps more translational ordering of the $F_8H_{11}PA$ SAM on the amorphous alumina.

The pure hydrocarbon SAMs reported here yield advancing and static contact angles consistent with the expression of the $-CH_3$ group at the air/film interface.[10,44,52,53] The advancing and static angles reported here for water are close to those for $H_{16}PA$ on aluminum's native oxide[10] and $H_{16}PA$ applied to amorphous alumina through a spin-coat and heat procedure.[44] Once again, the receding water contact angle values in our study are lower than those in previous studies (by ~10°), suggesting a somewhat lower coverage of $H_{18}PA$ in this study. In general, the reduced contact angles in this study as compared to those in previous work on films formed on the native oxide of aluminum may result from lower SAM coverage on the amorphous and crystalline alumina surfaces driven by the lower reactivity of these surfaces relative to the native oxide of aluminum.

We note here a subtle difference in contact angles between $H_{18}PA$ on these substrates and what is typically observed for SAMs of long-chain alkanethiols on gold. Whereas the advancing water contact angles reported here are essentially identical to what has been reported for thiols on gold (110−115°), advancing hexadecane contact angles are significantly lower (50−52° for thiols,[50,51] 38−41° for our work). Data from the literature have shown that water has an advancing angle of ~113° for a methyl surface, whereas on a methylene surface it is reduced to only ~103°.[54,55] Hexadecane, however, has an advancing contact angle of ~51° on a methyl surface, whereas it wets a methylene surface. Consequently, hexadecane is a more sensitive probe of the methylene content of a surface than is water. Whereas our advancing angles indicate a mostly methyl-terminated surface, which is nearly the same as that of long-chain alkanethiols on gold, the hexadecane advancing contact angles indicate that there is some degree of additional methylene content at the surface in our $H_{18}PA$ on sapphire and amorphous alumina than there is for alkane thiols on gold, consistent with the notion that the coverage is somewhat lower. Lower contact angles may also indicate a higher tilt angle from the surface normal. Advancing hexadecane contact angles with our $F_8H_{11}PA$ (80−81°) very nearly reproduce measurements of partially fluorinated thiols from the literature (e.g., 79° for F_8H_2SH[13] and 83° for F_8H_8SH[56]).

The PA SAMs are favorable to thiols in terms of longevity and stability. Whereas thiols on gold and silver oxidize and degrade with time in a matter of weeks,[57] the PA SAMs examined here were stable for the six months that elapsed between deposition and final AFM imaging; during that time, they were stored in an ambient laboratory atmosphere. The substrates were eventually reused for infrared spectroscopy measurements on the SAMs, so the maximum lifetime of these alumina/PA SAM pairs has not yet been determined.

B. Nanotribology of Bare versus Coated Samples. As expected, coating alumina surfaces with PA SAMs reduces friction (both in absolute force and differential friction α) at the single-asperity level, and the reduction is dramatic. This clearly demonstrates the effectiveness of PA SAMs in reliably reducing friction at the single-asperity level compared with uncoated substrates. In general, the reduction in friction may be due to both the reduced wettability of the sample and the reduced attractive normal and tangential interactions with the tip that the chemically inert methyl or trifluoromethyl groups express at the surface.

Interestingly, the reduction in pull-off force in going from bare amorphous alumina to PA SAM-coated alumina is very modest compared to the reduction in friction. We therefore attribute the friction reduction exclusively to a lower barrier to sliding and eliminate any decrease in contact area or attraction between the tip and sample as a possible cause for the reduced friction.

The low friction behavior persisted over the 6 months that the samples were studied, indicating far better tribological stability than for thiols on gold or silver.[6,57] The range of values of the work of adhesion, 0.040−0.12 J/m^2, is comparable to other measurements for silicon tips on SAMs[58] and includes the value measured for self-mated CH_3-on-CH_3 interfaces,[59] 0.060 J/m^2.

The reduced friction of bare amorphous alumina as compared to that of bare annealed sapphire seen in Figure 9 suggests that there is an increased amount of passivating adventitious carbon adsorbed from ambient exposure on the former. Nevertheless, the addition of the PA SAM still reduces differential friction by a factor of at least 5 beyond the lubrication provided by such contamination.

C. Effect of Fluorination on Nanotribology. In comparing different PA SAM films with each other, the most noticeable contrast is the pronounced increase in differential friction α in going from $H_{18}PA$ to $F_8H_{11}PA$ monolayers. Typically, there was also greater absolute friction at positive loads for the F_8H_{11} PA, with variations in adhesion resulting in outlying high absolute friction measurements for $H_{18}PA$, as seen, for example, in Figure 10. This is in agreement with previous results from other experimental and molecular dynamics studies of alkanethiols on gold,[14,60−63] although in these studies only the terminal group was fluorinated whereas the rest of the chain was strictly alkane. Here, the slope of the friction vs load data differed by a factor of ~1.5−3.6, depending on the substrate, whereas previous work on alkanethiols reported factors of 3 to 4. We note that our work is the first where friction and load forces are experimentally calibrated *in situ*.

The difference in friction between pure alkanes and $-CF_3$-terminated alkanes has been attributed previously to the greater size of the terminal CF_3 groups compared to that of CH_3 groups. Because only the terminal group was fluorinated in the previous studies, the packing densities of the two types of chains were identical, and equal numbers of large CF_3 groups were packed into the same area as CH_3 groups, imposing a significant barrier to CF_3 group motion (i.e., deformation and rotation). In the MD simulations of self-mated SAM interfaces by Park et al.,[60] this leads to higher ordering of the CF_3 groups in the film, and this is correlated with higher frictional forces. However, in our case, the top 8 out of 19 carbons are fluorinated, precluding such a direct comparison of the data. A different possible origin of this contrast is discussed further below.

(52) Bain, C. D.; Troughton, E. B.; Tao, Y. T.; Evall, J.; Whitesides, G. M.; Nuzzo, R. G. *J. Am. Chem. Soc.* **1989**, *111*, 321−335.
(53) Liakos, I. L.; Newman, R. C.; McAlpine, E.; Alexander, M. R. *Surf. Interface Anal.* **2004**, *36*, 347−354.
(54) Atre, S. V.; Liedberg, B.; Allara, D. L. *Langmuir* **1995**, *11*, 3882−3893.
(55) Allara, D. L.; Atre, S. V.; Elliger, C. A.; Snyder, R. G. *J. Am. Chem. Soc.* **1991**, *113*, 1852−1854.
(56) Weinstein, R. D.; Moriarty, J.; Cushnie, E.; Colorado, R., Jr.; Lee, T. R.; Patel, M.; Alesi, W. R.; Jennings, G. K. *J. Phys. Chem. B* **2003**, *107*, 11626.
(57) Leggett, G. J. *Anal. Chim. Acta* **2003**, *479*, 17−38.
(58) Burns, A. R.; Houston, J. E.; Carpick, R. W.; Michalske, T. A. *Phys. Rev. Lett.* **1999**, *82*, 1181.
(59) Thomas, R. C.; Houston, J. E.; Crooks, R. M.; Kim, T.; Michalske, T. A. *J. Am. Chem. Soc.* **1995**, *117*, 3830−3834.
(60) Park, B.; Lorenz, C. D.; Chandross, M.; Stevens, M. J.; Grest, G. S.; Borodin, O. A. *Langmuir* **2004**, *20*, 10007−10014.
(61) Kim, H. I.; Graupe, M.; Oloba, O.; Koini, T.; Imaduddin, S.; Lee, T. R.; Perry, S. S. *Langmuir* **1999**, *15*, 3179−3185.
(62) Graupe, M.; Koini, T.; Kim, H. I.; Garg, N.; Miura, Y. F.; Takenaga, M.; Perry, S. S.; Lee, T. R. *Colloids Surf., A* **1999**, *154*, 239−244.
(63) Kim, H. I.; Koini, T.; Lee, T. R.; Perry, S. S. *Tribol. Lett.* **1998**, *4*, 137−40.

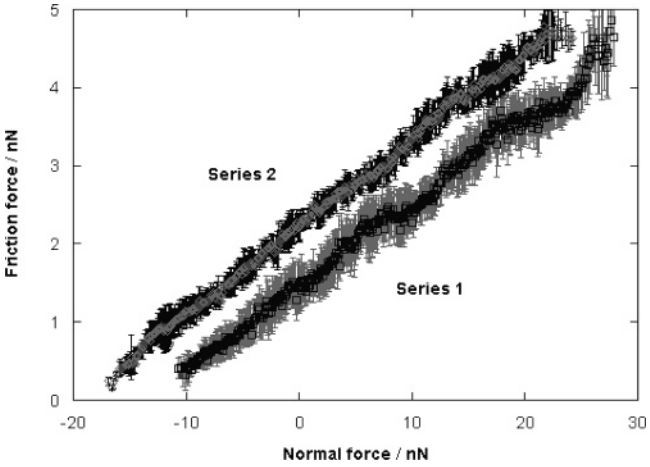

Figure 12. F_8H_{11} friction data at two nearby locations. 95% confidence intervals, $N = 5$.

D. Linearity of Friction versus Load. Several previous studies have reported that single-asperity frictional forces are often proportional to the true area of contact,[35,58,64−78] which for a single parabolic asperity between homogeneous, isotropic, linear, elastic materials, as well as in many other cases, varies in a nonlinear fashion with the load in a characteristic, well-defined manner.[79] This type of load dependence was rarely seen over the course of these experiments, as the individual FL plots typically were almost always highly linear, as seen in Figures 10 and 12.

Furthermore, consistent with the adhesion measurements described above, the FL measurements exhibit a local variation in the pull-off force (Figure 12). After FL measurements were performed at one position, the cantilever was moved to another spot, and another series was performed. Whereas the pull-off force increased by 50% from one position to another, the average differential friction α varied by less than 5%, validating the use of α as the figure of merit for comparing friction measurements. We believe that the consistency in this figure, despite the variations in absolute frictional force and adhesion force, is a rather remarkable demonstration of independent contributions to the total frictional behavior of an interface.

The linearity in the friction vs load data and the lack of dependence of α on the pull-off force can be explained by one of two hypotheses: (1) the shear strength is pressure-dependent or (2) friction is dominated by molecular plowing. The first hypothesis is motivated by the observation that single-asperity contacts demonstrate frictional forces F proportional to the interfacial shear strength τ and the true contact area A (i.e., $F = \tau A(L)$[80]). Expressing the shear strength dependence on the mean normal contact pressure to first order[12] yields $\tau = \tau_0 + \alpha L/A$ and therefore $F = \tau_0 A(L) + \alpha L$. When the second term dominates, FL plots are nearly linear. Thus, α represents the shear strength's dependence on mean contact pressure and is the figure of merit for friction. Because the AFM measures the response of the normal and shear contact stresses averaged over the entire tip-sample junction, and because the contact area drops out of the force equations above, this analysis of α is independent of the length scale of the contact (i.e. the radius of the tip). This may not be the case in general, especially for large ranges of tip radius and normal load.

This linear dependence has been suggested to be a manifestation of the Eyring activation model,[12,81−83] whereby the effect of increased normal contact pressure is to modify the conformation of the materials at the interface and to correspondingly create a larger energy barrier to sliding, thus increasing the frictional force per area (interfacial shear strength). This is expected to be a significant effect for softer materials such as polymers and SAMs, where pressure readily induces changes in the molecular conformation at the interface. However, for solids, where no such conformational change with applied pressure occurs, the interfacial shear strength remains constant as the pressure is increased, as long as the materials are only elastically deformed. Hence, the observation of linear FL behavior may be indicative of the fact that conformational changes, such as gauche defects, are being induced to an increasing degree as the load is increased, and this increases the shear strength. This is precisely what is observed in a recent molecular dynamics simulation of friction sliding for alkane-based SAM-coated surfaces.[84]

The second hypothesis is of a significantly different physical origin. Unlike two stiff solids sliding against each other, such as bare SiO_2 and Al_2O_3, the SAM layers are compliant and anisotropic on the atomic scale. Weak van der Waals forces between adjacent chains mean that displacements normal to the surface are localized (i.e., decoupled from their neighbors). Thus, one would not expect the SAM to be deformed as significantly outside of the contact region as an isotropic elastic solid would. However, the monolayer is densely packed in-plane, so lateral (shear) deformation will couple to molecules beyond the contact zone. If the compressive normal (vertical) deformation is localized only to the molecules immediately underneath the tip, then the act of sliding involves molecular-scale plowing. Because the tip lies below the top surface of neighboring PA molecules (Figure 13), the tip must either compress or laterally deform adjacent molecules in the forward direction to slide. As the load increases, the tip penetrates the monolayer by an increasing amount and encounters a greater physical barrier to motion because it must deform more material at high loads than low loads. From geometry, when a paraboloidal tip penetrates a flat surface, the projected contact area A_P of the tip along an in-plane direction (that is, the area of a 2-D parabola of curvature $^1/_R$ up to height

(64) Carpick, R. W.; Ogletree, D. F.; Salmeron, M. *J. Colloid Interface Sci.* **1999**, *211*, 395−400.
(65) Singer, I. L., Pollock, H. M. *Fundamentals of Friction: Macroscopic and Microscopic Processes*. Kluwer: Dordrecht, The Netherlands, 1992.
(66) Singer, I. L. Solid Lubrication Processes. In *Fundamentals of Friction: Macroscopic and Microscopic Processes*; Singer, I. L., Pollock, H. M., Eds.; Kluwer: Dordrecht, The Netherlands, 1992; Vol. 220, p 237.
(67) Carpick, R. W.; Agraït, N.; Ogletree, D. F.; Salmeron, M. *Langmuir* **1996**, *12*, 3334−3340.
(68) Carpick, R. W.; Agraït, N.; Ogletree, D. F.; Salmeron, M. *J. Vacuum Sci. Technol., B* **1996**, *14*, 1289−1295.
(69) Luthi, R.; Meyer, E.; Bammerlin, M.; Howald, L.; Haefke, H.; Lehmann, T.; Loppacher, C.; Guntherodt, H.; Gyalog, T.; Thomas, H. *J. Vacuum Sci. Technol., B* **1996**, *14*, 1280−1284.
(70) Carpick, R. W.; Salmeron, M. *Chem. Rev.* **1997**, *97*, 1163−1194.
(71) Lantz, M. A.; O'Shea, S. J.; Welland, M. E.; Johnson, K. L. *Phys. Rev. B: Condens. Matter* **1997**, *55*, 10776−10785.
(72) Lantz, M. A.; O'Shea, S. J.; Welland, M. E. *Phys. Rev. B: Condens. Matter* **1997**, *56*, 15345−15352.
(73) Johnson, K. L. *Proc. R. Soc. London, Ser. A* **1997**, *453*, 163.
(74) Enachescu, M.; van den Oetelaar, R.; Carpick, R.; Ogletree, D.; Flipse, C.; Salmeron, M. *Phys. Rev. Lett.* **1998**, *81*, 1877−1880.
(75) Carpick, R. W.; Enachescu, M.; Ogletree, D. F.; Salmeron, M. Making, Breaking, and Sliding of Nanometer-Scale Contacts. In *Fracture and Ductile vs. Brittle Behavior—Theory, Modelling, and Experiment*; Beltz, G., Kim, K.-S., Selinger, R. L., Eds.; Materials Research Society: Warrendale, PA, 1999; pp 93−103.
(76) Wei, Z.; Wang, C.; Bai, C. *Langmuir* **2001**, *17*, 3945−3951.
(77) Piétrement, O.; Troyon, M. *Langmuir* **2001**, *17*, 6540−6546.
(78) Piétrement, O.; Troyon, M. *Surf. Interface Anal.* **2001**, *31*, 1060−1067.
(79) Johnson, K. L. *Contact Mechanics*. Cambridge University Press: Cambridge, U.K., 1985; p 452.
(80) Carpick, R.; Agrait, N.; Ogletree, D.; Salmeron, M. *J. Vacuum Sci. Technol., B* **1996**, *14*, 1289−1295.
(81) Eyring, H. J. *J. Chem. Phys.* **1935**, *3*, 107.
(82) Eyring, H. J. *J. Chem. Phys.* **1936**, *4*, 283.
(83) McDermott, M. T.; Green, J. B. D.; Porter, M. D. *Langmuir* **1997**, *13*, 2504−2510.
(84) Tutein, A. B.; Stuart, S. J.; Harrison, J. A. *Langmuir* **2000**, *16*, 291−296.

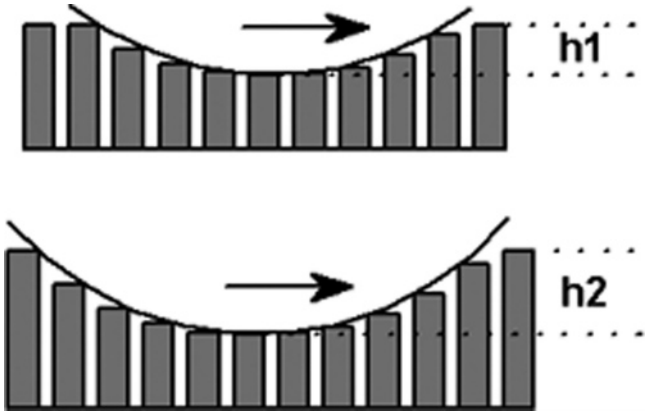

Figure 13. van der Waals interaction between the chains is weak, allowing individual molecules to deform independently along their vertical axes. The AFM tip therefore compresses molecules locally, penetrating the original surface plane of the film by a depth *h*. Some degree of plowing is required for lateral motion, requiring compressing or laterally deforming molecules in the forward neighboring direction over the penetration depth. The work required to slide laterally is proportional to the work required to compress or laterally deform the forward neighboring molecules. Tip penetration is greater at high loads (h2) than low loads (h1), and the shear strength of the interface increases with load.

h) is proportional to $\sqrt{Rh^3}$. For a contact that is Hertzian or weakly adhesive (such as a DMT contact), the normal load L associated with the penetration depth h is $L = {}^4/_3 E^* \sqrt{Rh^3}$, where E^* is the reduced modulus of the contact.[79] Therefore, the projected area A_P is proportional to ${}^L/_{E^*}$ and independent of R. Furthermore, an increase in adhesion simply adds to the total load, and the linear dependence between the total load and projected contact area remains the same. If we postulate that plowing dominates over interfacial sliding (i.e., that friction is proportional not the to in-plane tip−surface contact area but to the contact area projected onto the vertical plane), then $F = \tau_p A_p$ and friction will be linearly proportional to the load. The physical basis for this postulate is that frictional energy dissipation is not due to the sliding of molecules past one another at the contact interface but to the mechanical deformation of the forward neighboring molecules. This is essentially a molecular-scale manifestation of viscoelasticity: a portion of the energy expended to deform the molecules mechanically (in this case, to allow the tip to move forward) is not recovered but is instead dissipated.

It is not possible, without further complementary experiments and perhaps detailed simulations, to determine which, if either, of the two hypotheses described above applies here. However, it is clear that the simple model of interfacial friction for single asperities, where friction is proportional to the contact area and a constant interfacial shear strength, does not apply here and that the slope of the FL curve is a key indicator of the mechanism of frictional energy dissipation.

E. Effect of the Substrate on the Nanotribological Response. Epitaxial effects are believed to be the cause of the more subtle but nonetheless reproducible dependence of friction upon the substrate for both PA SAMs. Using the van der Waals radii values of Tamada,[17] lower bounds of the surface areas required per CH_2 and CF_2 chain are 0.156 and 0.278 nm^2, respectively. This means that the H_{18}PA chain is smaller in cross section than the repeating surface area of the two crystalline alumina substrates (0.196 and 0.244 nm^2 for C and R, respectively), so the availability of packing sites for H_{18}PA chains should be the limiting factor for packing density and the C-plane should support a denser coating. Additionally, the O−O distances in the sapphire basal plane (0.27 nm) are very close to the spacing of the single-bonded terminal O's of the phosphonic acid group (0.28 nm) as calculated by Chem3D (CambridgeSoft Corp., Cambridge, MA) (Figure 14, which shows the entire molecule, with the headgroup in the foreground). Thus, a (1 × 1) epitaxial relationship between the H_{18}PA headgroups and the C- and R-plane unit cells is likely and would lead to a nearly ideally packed monolayer on the former and a less dense monolayer on the latter (Figure 15). The lower density would lead to a larger tilt angle of the molecules. The reduced friction that we observe for the C plane compared with that for the R plane of the H_{18}PAs is therefore consistent with previous reports of increased packing density of alkanethiol SAMs correlating with a reduction in friction.[83−86] Furthermore, a comparison of the friction data between the R-plane and amorphous alumina suggests that, on average, surface bonding sites are closer together in the aperiodic distribution of the latter than in the R-plane of sapphire and are comparable to that of the C-plane.

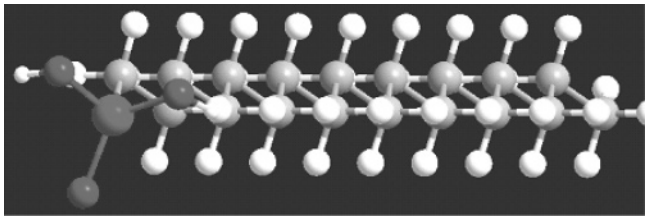

Figure 14. End-on view of an entire isolated PA molecule, showing the tetragonal arrangement of the O and P atoms in the headgroup. The headgroup is on the left, in the foreground.

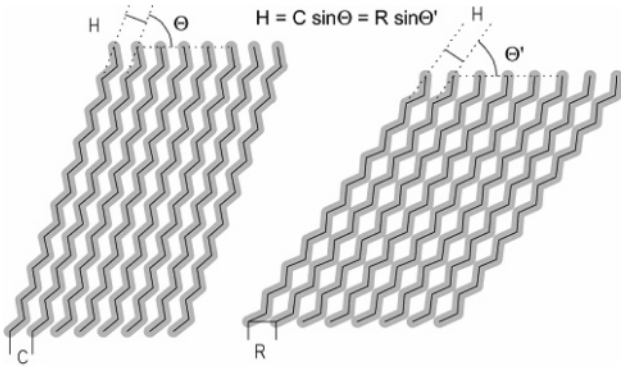

Figure 15. Packing of H_{18}PA on C and R planes of sapphire, assuming (1 × 1) epitaxy. The chains maintain the equilibrium van der Waals spacing (denoted H) for both surface meshes by changing the tilt angle according to the surface bonding site density.

However, a single F_8H_{11}PA chain requires more area (0.278 nm^2) than either repeating surface mesh for the C and R planes, preventing an ordered (1 × 1) epitaxial arrangement of the PA molecules; the SAM molecules are simply too large for efficient (1 × 1) packing on the crystalline surfaces. The next largest repeating surface units, ($\sqrt{2} \times \sqrt{2}$) for R and ($\sqrt{3} \times \sqrt{3}$) for C, are large enough for a CF_3 chain but at a less-than-ideal packing density. Also, each F_8H_{11}PA molecule has two diameters competing to determine the packing order, with the longer hydrogenated section seeking a much closer packing with its neighbors via van der Waals interactions than the bulkier fluorinated section can accommodate. Figures 16 and 17 demonstrate how the F_8H_{11}PA monolayers may organize on the C and R planes when either the CH_2 or CF_2 segments dominate the packing, respectively.

(85) Lee, S.; Shon, Y. S.; Colorado, R.; Guenard, R. L.; Lee, T. R.; Perry, S. S. *Langmuir* **2000**, *16*, 2220−2224.
(86) Lio, A.; Charych, D. H.; Salmeron, M. *J. Phys. Chem. B* **1997**, *101*, 3800−3805.

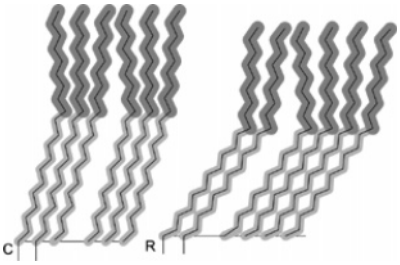

Figure 16. Packing of F_8H_{11} SAMs on the C and R planes of sapphire for the case where the CH_2 segments dominate, maintaining equilibrium spacing. Fluorinated portions of the chain are distorted.

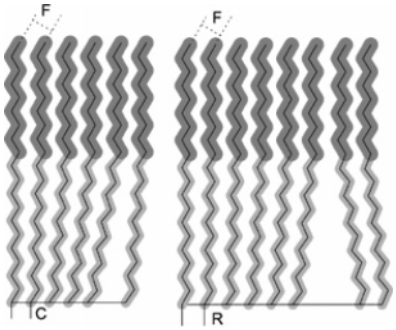

Figure 17. Packing of F_8H_{11} SAMs on the C and R planes of sapphire for the case where the CF_2 segments dominate, maintaining equilibrium spacing. Hydrogenated portions of the chain are distorted. F, C, and R represent the repeat distances for CF_3 packing and unit meshes of C/R plane sapphire.

Frey et al.[47] have studied this topic using similar molecules: $F_{10}H_2$, $F_{10}H_{11}$, and $F_{10}H_{17}$ alkanethiols, using Au and Ag substrates to dictate surface periodicity. There, the surface mesh was also larger than the CH_2 segments and smaller than the CF_2 segments. The absolute tilt angle of the CF_2 chains (relative to the surface normal rather than the CH_2 segments) was not affected by the substrate but did increase with the number of CH_2 segments. Longer molecules had more CH_2-CH_2 van der Waals interactions and behaved more like unfluorinated thiols. On the basis of the results of that paper, we believe that the F_8H_{11}PA SAM's packing structure is closer to that at the end of the spectrum where CH_2 segments dominate (Figure 16). Although the question of how the CH_2 and CF_2 segments accommodate each other depending on substrate crystallinity is an interesting one, this discussion should not detract from our conclusion that the small size of the surface meshes relative to the size of the CF_2 groups imposes a suboptimal packing arrangement. The amorphous alumina, however, does not necessarily impose poor registry between the bonding sites and the PA molecules.

Comparing the friction data for F_8H_{11}PA on amorphous alumina with F_8H_{11}PA on crystalline alumina, we therefore conclude that the packing density is somewhat greater on the former, resulting in the observed reduction in friction. The differences in contact angle measurements between amorphous and crystalline substrates for the fluorinated films indicate greater packing density on the amorphous surfaces, bolstering this conclusion.

There is another explanation for F_8H_{11}PA having lower friction on the amorphous substrate. Molecular dynamics simulations[87,88] have linked higher interfacial ordering and commensurability with higher friction. This implies that these monolayers retain the order of the substrates, despite the incommensurability of the SAM and crystal. If this is the case, then it would come at the cost of reduced packing density.

Conclusions

Static and advancing contact angle measurements performed with water and hexadecane are consistent with previous reports of PA SAMs on aluminum oxide substrates, showing that both H_{18}PA and F_8H_{11}PA SAMs render alumina surfaces highly hydrophobic. However, receding measurements here are generally lower with these samples, suggesting that somewhat lower coverage is attained here than previously reported.[10,44] The contact angle data also suggests that F_8H_{11}PA has a somewhat higher packing density and/or ordering on the amorphous substrate compared to that of the crystalline substrates. The topographic and tribological properties of the SAMs were stable in a laboratory environment for at least 6 months, indicating their high degree of ambient environmental stability, which is far greater than that for alkanethiols.

AFM topographs show that PA SAMs on annealed sapphire and vapor-deposited alumina are smooth and uniform. Loosely bound contaminants or nonbonded PA molecules that were not removed by an ethanol rinse are observed for films on R-plane sapphire, and these are readily swept aside during contact mode AFM scanning to reveal the atomic steps of the underlying single crystal sapphire substrate. Contamination of the tip by the monolayer is observed for all films, leading to transient effects in nanotribology measurements unless the tip and sample are brought to a steady state via a run-in process that we believe coats the tip with a defective layer of PA molecules. Our interfaces can therefore be considered to be nearly self-mated, but experiments with tips deliberately coated with SAMs in a deposition process will be required to verify this hypothesis.

Adhesion between PA SAMs and processed silicon AFM tips is influenced by partial fluorination, and friction is influenced both by fluorination and the surface arrangement of the alumina substrate. Specifically, adhesion between processed tips and F_8H_{11}PA ranged from 50 to 100% of that for H_{18}PA and was never larger. The force−distance technique of adhesion measurement consistently yielded reduced values of the pull-off force compared with those from the friction versus load technique. The compression of chains on the tip and sample resulting from more vigorous contacts between the two in the latter method may be the cause of this effect, along the lines of previous reports of adhesion hysteresis.

Both types of SAMs demonstrated a large reduction in friction compared with the friction of all bare alumina substrates. Furthermore, single-asperity friction coefficients for fully hydrogenated SAMs were consistently less, by 40−70%, than the corresponding values for semifluorinated SAMs. Also, the linear nature of the friction versus load measurements indicates that either the interfacial shear strength is pressure-dependant, or that friction is governed by the plowing of the tip through greater depths of the SAM with increasing load.

Whereas applying SAMs greatly reduced the friction for all substrates, some trends within a given SAM type indicate a second-order effect arising from the choice of alumina substrate. Friction is generally lower for amorphous substrates than crystalline ones, whereas differentiation between the C and R planes suggests that steric and epitaxial effects play a small but observable role in the packing and subsequent frictional response of the SAMs.

Acknowledgment. This work was supported by the National Science Foundation (CAREER Award No. CMS-0134571).

LA052847K

(87) Chandross, M.; Webb, E. B.; Stevens, M. J.; Grest, G. S.; Garofalini, S. H. *Phys. Rev. Lett.* **2004**, *93*, 166103.

(88) Muser, M. H.; Wenning, L.; Robbins, M. O. *Phys. Rev. Lett.* **2001**, *86*, 1295−1298.